Filamentation of the plasma expanding from a laser-irradiated solid

Contact kquinn09@qub.ac.uk

K. Quinn, B. Ramakrishna, C. A. Cecchetti, L. Romagnani, G. Sarri, P. A. Wilson and M. Borghesi
Centre for Plasma Physics, Queen's University Belfast, Belfast, BT7 1NN

R. J. Clarke, P. Gallegos, D. Neely and M. Notley
Central Laser Facility, STFC, Rutherford Appleton Laboratory, HSIC, Didcot, Oxon OX11 0QX, UK

A. Macchi
CNR/INFM, Dipartimento di Fisica "E. Fermi," Pisa, Italy

D. C. Carroll, M. N. Quinn, X. H. Yuan and P. McKenna
SUPA, Department of Physics, University of Strathclyde, Glasgow G4 0NG, UK

L. Lancia and J. Fuchs
LULI, École Polytechnique-Université Paris VI, 91128 Palaiseau, France

Introduction

A number of instabilities may develop in the plasma created by the interaction of a short pulse, high intensity laser with a medium. These include (but are not limited to) the Weibel [1], two-stream [2], current filamentation [3], and electro-thermal [4] instabilities. As yet, a cohesive picture of the relationship between each instability, and their spatial and temporal effects on a plasma, has yet to be completed, yet studies of such instabilities in the laboratory can inform the mechanisms behind a number of astrophysical phenomena [5]. Moreover, the development of laser-driven ion [6] and fusion energy [7] sources requires increased understanding of the complex physics surrounding the intense laser-matter interaction.

In the paragraphs that follow, we describe the highly-regular and stable instabilities observed following the incidence onto a metallic wire target of a mid-10^{19} W/cm^2 laser pulse. A model for the persistence of the observed filaments over ~100 ps timescales is proposed, whilst the initial mechanism by which they are seeded in the plasma expanding from the wire is tentatively attributed to either a current filamentation or electro-thermal instability.

Proton radiography

The data were obtained using the well-established proton radiography (or proton projection imaging) diagnostic [8]. In this scheme, the proton beam produced in the interaction of a high-intensity laser pulse with a thin metallic foil via the Target Normal Sheath Acceleration (TNSA) mechanism [6] is used to probe the electromagnetic fields induced by the interaction of a secondary pulse with the target of interest. Such TNSA-driven proton beams are intrinsically highly laminar, collimated, divergent, and broadband in energy.

Beyond the interaction target lies the transverse detector which typically takes the form of a layered stack of radiochromic films (RCFs). RCF [9] is an absolutely-calibrated dosimetry medium which responds to ionising radiation. Protons of the probe beam will suffer Lorentz deflections under the action of the E- and B-fields set up in the region of the interaction target. The resulting modulations to the transverse proton density of the beam can hence be observed at the RCF stack.

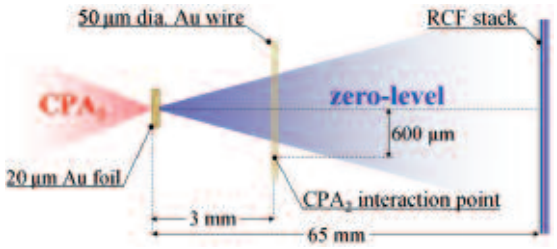

Figure 1. Experimental setup. CPA_2 strikes into the page.

A freely-available Monte Carlo code [10] may be used to compute the stopping distance of a proton traversing a thickness of RCF as a function of its energy. In this way, the proton signal observed on each layer of the detector stack may be related to a corresponding proton energy E_p. If the distance from the proton source to the interaction target is d, then by time-of-flight, this energy resolution of the detector corresponds to an intrinsic temporal resolution of the diagnostic, and the probing time associated to a given layer in the stack may be written $t_{probe} = d\,(m_p/2E_p)^{1/2}$ where m_p is the proton mass.

Experiment

The experiment was conducted in TAP [11], the principal target area for the Vulcan laser at the Rutherford Appleton Laboratory. Inside the target chamber, some 10% of the beam energy was diverted using an infrared pickup mirror to provide the interaction pulse (CPA_2). The remaining 90%, meanwhile (CPA_1), was focused onto a gold foil to produce the proton beam for probing of the interaction. Typical probe beam cut-off energies of 40 MeV were observed.

On a particular shot, the 600 fs-duration, 6×10^{19} W/cm^2 CPA_2 interaction pulse was incident upon a 50 μm-diameter gold wire target. A schematic of the experimental setup is shown in Fig. 1.

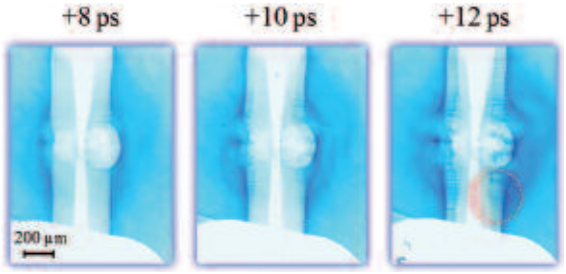

Figure 2. RCF images describing filament development following the CPA_2 interaction. The laser is incident on the centre of the wire from the right. The times associated to each RCF layer are expressed relative to the arrival time of the 0.6 ps-duration CPA_2 pulse. An enlarged version of the region highlighted in the right-most image is shown in Fig. 3(i).

A relative delay was introduced between the incidences of CPA_1 and CPA_2 onto their respective targets to ensure that the target wire was completely enveloped in the probe beam at the time of the interaction. In this way, information on times before, during, and up to 50 ps after the arrival of the CPA_2 interaction pulse was recorded at the detector.

In the immediate wake of the interaction, the proton density modulations visible on the RCF data obtained describe the ultrafast charging of the target wire, behaviour which has been proven to be the result of the escape of a small fraction of the laser-accelerated hot electron population to vacuum [12]. As shown in Fig. 2, however, highly-ordered filamentary structures appear normal to the wire surface all along its length in the RCF image corresponding to a probing time 10 ps after the arrival of CPA_2. We observe a regular oscillation between areas of high and low proton density (i.e. between darker and lighter regions on the RCF, respectively) suggesting that the quasi-static field structure responsible for the observed proton deflection pattern must have been somehow modulated in space also.

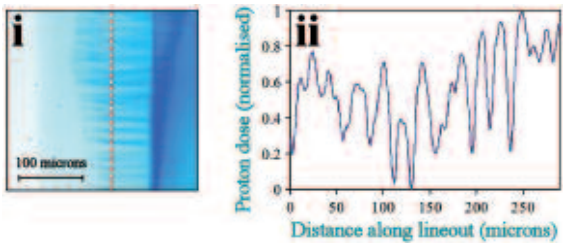

Figure 3. (i) Enlarged version of the region highlighted in the right-most image of Fig. 2. (ii) Proton density lineout taken along the dotted red line of the RCF shown.

In Fig. 3, we clearly see the remarkable periodicity of the filamented plasma surrounding the wire. The average wavelength of the oscillatory deflection pattern on the RCF may be measured to be ~20 μm. Examination of the full RCF data set reveals the filaments to be highly stable in time, maintaining their appearance wavelength and persisting for ~100 ps after the time of their formation. As time passes, meanwhile, the filaments expand outwards from the wire surface in the radial direction. Significantly, their presence is limited to the region within the wire plasma created by the CPA_2 interaction, strong evidence that the observed instability is not seeded by the interaction between the laser-driven hot electrons and the residual gas in the target chamber, and that the wire plasma itself plays a role in its formation.

Modelling a filament tube

We will now consider a possible mechanism for the formation of an individual filament tube. Note that in the following discussion, the perturbation leading to the creation of a filament is introduced at the wire surface; the filament itself will be formed as the quasi-static fields produced by this perturbation expand outwards in the radial direction along with the quasi-neutral wire plasma inside which they are held.

Of the hot electrons accelerated by the CPA_2 interaction with the target, only a small percentage above a threshold energy may escape to vacuum. The remainder will be attracted back towards the target under space-charge separation forces. To maintain global charge neutrality in the system, this hot electron current must be balanced by an equal and oppositely-flowing cold return current. From Ampère's Law:

$$\oint_C \mathbf{B} \cdot d\ell = \mu_0 I_{enclosed}$$

we see that the formation of magnetic field B requires the flow of a net current $I_{enclosed}$ through the closed loop under consideration C. On the local level, however, the hot and cold electron currents may not necessarily be uniform in space – if we consider the magnetic field associated with individual moving electrons in this picture, it can be shown that the development of highly ordered current flow is possible [3]. One possible configuration, then, for the seeding of this instability could be for the hot electron current returning to the wire to be localised in the centre of an imaginary tube. The radial distance r from the tube axis by which the net hot electron current flowing in towards the wire is neutralised by the net cold return current flowing outwards in turn defines the radius of the filament, r_{fil}.

Applying Ampère's Law to an individual filament tube, we see that there must be zero azimuthal magnetic field B_φ at $r = 0$ and at $r = r_{fil}$. The precise rise and decay of B_φ in the intervening space depends on the specific distributions of the hot and cold electron currents, though as an approximation, we will assume sinusoidal behaviour in this region (see Fig. 4). Experimentally, we observe the filaments to be highly stable, so that the electromagnetic fields associated to them may be assumed to be quasi-static. By using some simple magneto-hydrodynamic reasoning, then [13], the local gradient in plasma pressure required to balance the pinching action of B_φ may be written:

$$\nabla p = -\left(\frac{1}{2\mu_0}\frac{\partial B_\phi(r)^2}{\partial r} + \frac{B_\phi(r)^2}{\mu_0 r}\right)$$

where μ_0 is the permeability of free space. The radial E-field resulting from such a pressure gradient may in turn be computed by:

$$E = -\frac{\nabla p}{en}$$

where e is the elementary charge and n is the local plasma density.

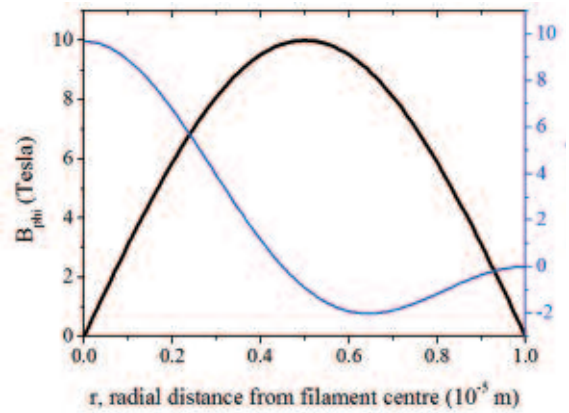

Figure 4. Graph displaying the profile of the pinching magnetic field across a filament B_φ and the related change in plasma pressure *dp* required to hold the system in equilibrium.

Possible distribution 1: column of filaments

Fig. 5 describes the simplest distribution of filaments on the wire surface that might result in the observed RCF deflection pattern of Fig. 3(i). In this picture, the laser will have come from the +*z* direction. The probe proton beam, meanwhile, is centred on the *x*-axis whilst the filament column runs along *y*.

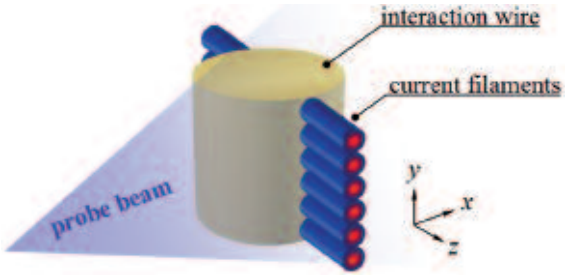

Figure 5. Schematic describing the proton probing of a column of filament tubes.

This possible filament configuration was studied using 3D particle tracing simulations. By comparing the simulation results with the experimental RCF data obtained, the validity of the proposed filament configuration may hence be gauged.

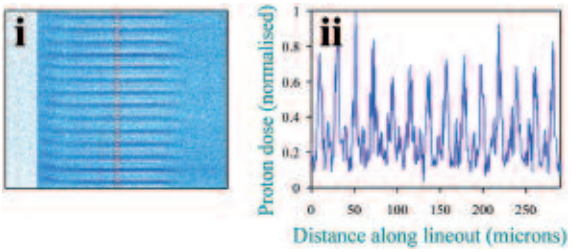

Figure 6. (i) Proton density map produced by a three-dimensional particle tracing simulation which considered the filament configuration described by Fig. 4. (ii) Proton density lineout taken along the dotted red line of the simulated RCF shown.

The simulation output of Fig. 6(i) was obtained by assuming a peak value for B_φ of 10 T and a background plasma density of 10^{17} cm^{-3}. The filament wavelength/separation was set to 20 μm. Whilst there is undeniable similarity between the experimental (Fig. 3) and simulated (Fig. 6) RCF images, the discerning reader might question the arrangement of the observed current filaments into such a highly-ordered state.

Possible distribution 2: random filament placement

Particle tracing simulations similar to those described by Fig. 5 were carried out in which filament tubes were placed at random on the surface of the wire. More precisely, both the *y* and $\varphi = \tan^{-1}(x/z)$ coordinates used to define the centre of each filament were randomly selected. In this fully-3D configuration, the average filament separation λ_{av} may be determined by $\lambda_{av} = (A/N)^{1/2}$ where *A* is the surface area simulated and *N* is the number of filaments. The particle tracing output of Fig. 7 was produced by assuming an average filament separation of λ_{av} = 30 μm, a peak B_φ value of 0.3 T, and a background plasma density of 10^{16} cm^{-3}. The simulated RCF image of Fig. 7 is undoubtedly comparable to, if slightly "messier" than, the experimental RCF image of Fig. 3. Perhaps the true filament distribution on the surface of the wire is somewhere in between the highly-ordered "column of filaments" distribution proposed and this completely randomly-generated distribution.

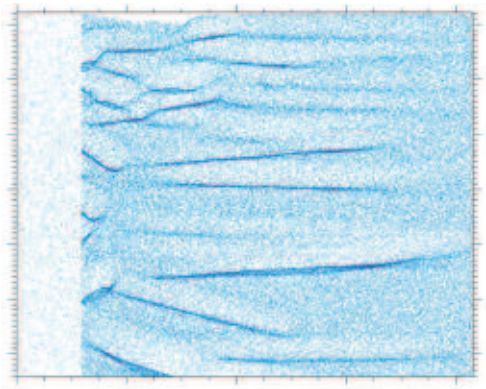

Figure 7. Output from a particle tracing run which considered the filaments to be placed randomly on the wire surface.

Dependence of filament wavelength on target material

Additional shots were performed at comparable pulse intensities for 100 μm-diameter wires of varying atomic number, Z. As described by Fig. 8 below, smaller RCF deflection pattern wavelengths are obtained for wire materials of higher-Z.

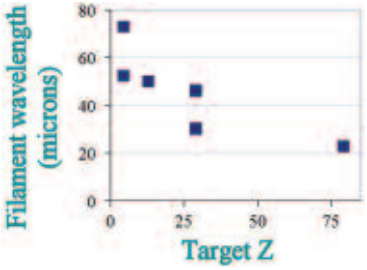

Figure 8. Average filament wavelength as a function of target atomic number, Z.

This Z-dependence of the wavelength of the filamentary structures produced in the interaction between counterstreaming hot and cold electron flows was predicted almost three decades ago[4]:

$$\lambda = \frac{2\pi}{k} = 2.41 \times 10^{10} \frac{T_e^{\ 2} A^{1/2}}{n_0 Z y^{1/2}}$$

Perhaps it is not entirely unreasonable to draw from this that, at the time of its formation, a single filament may have a saturation electron current beyond which no further flow may be supported in a given direction. In this framework, a greater abundance of cold electrons in the wire plasma supplying the required return current will result in the need for a larger number of filaments per unit area on the target surface.

Summary

The filamentation of the plasma expanding from a wire irradiated by a high-intensity, short-pulse laser has been studied via proton radiography.

In all shots performed, the onset of filamentation is observed to occur in the wake of the ps-duration interaction pulse. The observed structures demonstrate remarkable spatial regularity, and are very stable in time, remaining intact for long (~100 ps) after the time of their formation. Possible configurations for the observed filaments have been proposed on the basis of the results of a series of particle tracing simulations.

The spatial separation of the observed structures has shown strong dependence on the atomic number of the wire target used, a theoretically-predicted behaviour for the case of a hot electron current being neutralised by a counterstreaming cold return current. As such, the data obtained may help in the development of our understanding of a number of phenomena in astrophysics, nuclear fusion, and laser-driven ion acceleration.

Acknowledgements

The author would like to acknowledge the support of the staff of the Central Laser Facility in the running of the experimental investigation described.

References

1. E. S. Weibel, *Phys. Rev. Lett*. **2**, 83 (1959).
2. A. Bret *et al*., *Phys. Rev. Lett*. **94**, 1150002 (2005).
3. F. Califano *et al*., *Phys. Rev. E*, **58**, 7837 (1998); G. Rowlands *et al*., *New Journ. Phys*. **9**, 247 (2007).
4. M. G. Haines, *Phys. Rev. Lett*. **47**, 917 (1981).
5. B. Remington *et al*., *Science* **284**, 1488 (1999).
6. M. Borghesi *et al*., *Fus. Sci. Tech*. **49**, 412 (2006).
7. A. Macchi *et al*., *Nucl, Fusion* **43**, 362 (2003).
8. L. Romagnani *et al*., *Laser Part. Beams* **26**, 241 (2008).
9. http://www.gafchromic.com
10. http://www.srim.org
11. C. N. Danson *et al*., *Nucl. Fusion* **44**, S239 (2004).
12. K. Quinn *et al*., *Phys. Rev. Lett*. **102**, 194801 (2009).
13. S. Pfalzner, *"An Introduction to Intertial Confinement Fusion"*, Taylor and Francis (2006).